Journal of The Electrochemical Society, **154** (5) A396-A406 (2007)
0013-4651/2007/154(5)/A396/11/$20.00 © The Electrochemical Society

CO Coverage/Oxidation Correlated with PtRu Electrocatalyst Particle Morphology in 0.3 M Methanol by In Situ XAS

Frances J. Scott,[a,z] Sanjeev Mukerjee,[b,*] and David E. Ramaker[a,*]

[a]*Department of Chemistry, The George Washington University, Washington, DC 20052, USA*
[b]*Department of Chemistry and Chemical Biology, Northeastern University, Boston, Massachusetts 02115, USA*

In situ X-ray absorption spectroscopy (XAS) measurements, including both X-ray absorption near edge spectroscopy (XANES) and extended X-ray absorption fine structure (EXAFS) at the Pt L_3 and Ru K edges, were carried out on three different carbon-supported PtRu electrocatalysts in an electrochemical cell in 1 M $HClO_4$ with 0.3 M methanol. The CO and OH adsorbate coverage on Pt and Ru were determined as a function of the applied potential via the novel delta XANES technique, and the particle morphology was determined from the EXAFS and a modeling technique. Both the bifunctional and direct CO oxidation mechanisms, the latter enhanced by electronic ligand effects, were evident for all three electrocatalysts; however, the dominant mechanism depended critically on the particle size and morphology. Both the Ru island size and overall cluster size had a very large effect on the CO oxidation mechanism and activation of water, with the bifunctional mechanism dominating for more monodispersed Ru islands, and the direct surface ligand effect dominating in the presence of larger Ru islands.
 [DOI: 10.1149/1.2709496]

Manuscript submitted August 14, 2006; revised manuscript received December 11, 2006. Available electronically March 12, 2007.

The search for alternate mobile power sources is currently targeted toward improvement in the performance of both reformate and direct methanol fed polymer electrolyte membrane (PEM) fuel cells. One primary goal is to increase the tolerance of the traditional Pt anode toward CO poisoning. Extensive research has been reported as recently reviewed by Marković and Ross.[1]

It has long been known that partially alloying the traditional Pt anode with another metal, resulting in some form of bimetallic electrocatalysts, can increase its CO tolerance and reduce the amount of costly Pt needed. Research has been conducted on both Pt–M bimetallic nanocrystals and M-decorated Pt single crystals involving Ru,[2-31] Mo,[18,19,21,22,32-35] Sn,[17,20,36-48] and other transition metals.[2,49-51] Pt–Ru catalysts have emerged as the most CO-tolerant catalysts for both the reformate and methanol fuels, depending upon the support.[52] Despite the wealth of research in this area, the reasons for the effectiveness of Pt–Ru over other alloys are still hotly debated.

Two widely accepted mechanisms for the oxidation of CO from the Pt–Ru surface exist.[10,15,16,38,53] The "bifunctional" mechanism involves activation of water at the Ru surface to yield Ru–OH

$$Ru + H_2O \rightarrow Ru\text{–}OH + e^- + H^+ \quad [1]$$

This hydroxide is tightly bound; however, the more mobile CO is assumed to migrate across the surface to react with this OH

$$Pt\text{–}CO + Ru\text{-}OH \rightarrow Pt + Ru + CO_2 + e^- + H^+ \quad [2]$$

In contrast, the direct mechanism, enabled by the ligand or electronic effect, holds that Ru modifies the electronic structure of the Pt by donating electron density, thus either weakening the Pt–CO bond and thereby allowing CO to be more easily oxidized directly by OH deposited on the Pt surface, or by enhancing Pt–H_2O activation and thereby allowing the reaction of OH and CO directly on the Pt. For single crystal Pt decorated by other metals, particularly for Ru on Pt(111), the bifunctional mechanism is generally acknowledged as the dominant effect.[11-14,25] However, the electronic effect has been suggested to provide the increased tolerance to CO in reformate systems, presumably by weakening the Pt–CO bond and decreasing the CO coverage, and thereby increasing the anode efficiency by leaving more surface sites free for H adsorption at low potential.[38] Additionally, the ligand effect has been shown to have a large effect on Pt atoms near Ru islands for Ru/Pt(111), but Pt atoms far from these islands are affected minimally.[4] Although the externally exposed Ru islands are known to be in some stage of oxidation in an aqueous electrode (i.e., RuO_nH_m at nearly all potentials),[54,55] for convenience we shall continue to designate these islands as Ru in this work.

The existence of two distinct regions of CO removal in cyclic voltammetry (CV) curves for Pt single crystals decorated by Ru has been found by several authors as summarized briefly in Table I. The two peaks have historically been attributed to earlier (lower potential) formation of OH/Ru, and thus removal of CO at or very near the Ru surface (the bifunctional mechanism), followed by OH production directly (the direct mechanism enabled by the electronic or ligand effect) on the Pt surface and removal of further CO.[56] Koper, Lebedeva, and Hermse,[11-14] on the other hand, propose that OH formed at the interface of the Ru islands on Pt(111) plays the dominant role, and that the second higher potential CO peak is due to slow diffusion of CO to the Ru/Pt interface (i.e., both peaks are attributed to the bifunctional mechanism, a fast and slow process, termed the BF fast and slow processes in Table I). Friedrich et al.,[57] using in situ infrared (IR) spectroscopy, found that both the CO/Ru and CO/Pt coverage decreased at the same potential and therefore also concluded that the BF mechanism dominated (the slow scans used to measure IR data make the slow and fast BF differentiation moot). In contrast, Lu et al.,[25] using chronoamperometry studies, concluded that the second peak arises from OH formation directly on the Pt, but near the Ru islands where the surface ligand effect is large, therefore termed the direct electronic mechanism (D in Table I) here. These studies were also able to show a slow and fast CO migration to the Ru interface, which broaden the D peak. Finally, Massong et al.,[32] using CV studies comparing Ru/Pt(111) and Ru/Pt(332), found that the doublet peaks were similar except for two aspects: (*i*) the Ru/Pt(332) second peak tailed off to higher potential much slower than for Ru/Pt(111) and (*ii*) the two peaks were shifted to lower potential by about 0.1 V. The shift to lower potential is known to arise from water activation (i.e., OH adsorption) at the more reactive steps and edges.[58-60] The slower tailing off was attributed to more strongly bound CO at these steps/edges, which cannot diffuse to the Ru islands, and therefore require direct OH adsorption at higher potential (the D mechanism).[32]

In this work, we shall distinguish three different mechanisms as summarized in Table I. The first region of CO removal is speculated to be due to the bifunctional mechanism involving formation of OH on the Ru islands, with subsequent CO diffusion and oxidation. The second region of CO removal is due to the formation of OH directly on the Pt surface, now enabled by the electronic or ligand mechanism with subsequent removal of CO from the Pt surface. However, we distinguish two regions of direct OH/Pt adsorption, that arising from Pt atoms near the Ru islands (hereafter "near Ru"), which

* Electrochemical Society Active Member.
z E-mail: fjscott@gwu.edu

Table I. Summary of proposed CO oxidation mechanisms and potential regions on PtRu.

	1st	2nd	3rd
Previous work			
Potential regions Ru/Pt(111)	<0.6 V vs RHE	0.6–0.7 V vs RHE	>0.7 V vs RHE
Koper et al.[11-14]	BF, fast	BF, slow	Preempted[a]
Friedrich et al.[32]		BF	
Lu et al.[28]	BF	D, fast and slow	Preempted
Potential regions Ru/Pt(332)	<0.5 V vs RHE	0.5–0.6 V vs RHE	>0.6 V vs RHE
Massong et al.[33]	BF	D	Preempted
This work			
Potential regions PtRu clusters	<0.25 V vs RHE	0.25–0.4 V vs RHE	>0.4 V vs RHE
Mechanism	BF	Dsl	Dil
PtRuE	Ineff.: poor PtRu interface and CO covered islands	Eff.: mobile CO on cluster faces and strong ligand effect	Eff.
PtRuW	Eff.: better PtRu interface and monodisperse Ru	Ineff.: Immobile CO at edges/corners, and reverse ligand effect	Eff.
Pt_3RuW	Partially eff.	Ineff.	Eff.

[a] All CO is removed by this point via the earlier two mechanisms.

experience a strong surface ligand effect (termed Dsl in Table I), and that arising from a weaker interior Ru atom ligand effect (termed Dil in Table I). Pt atoms "away from Ru" are primarily involved with the Dil mechanism. This latter mechanism is not at all active for Ru on single crystal Pt surfaces, because no Ru exists below the surface in this case and, in any event, it is preempted by the more effective BF mechanism.

Our supported PtRu nanoparticles have stronger CO–Pt bonds at the edges/corners compared to that on the plateaus or faces, and therefore this CO/Pt is not highly mobile. This requires the OH to be adsorbed near these Pt sites, but these sites are also much more reactive to water than Pt(111) sites, because of the interior Ru ligand effect, and the more reactive corner/edge sites. The more reactive corner/edge sites on nanoparticles shift all of the peaks down by about 0.1–0.2 V from even the stepped surface as shown in Table I. The relative infrequency of plateaus on Pt nanoparticles and the conditions under which the X-ray absorption near edge spectroscopy (XANES) data are taken in this work (like the IR data mentioned above), makes distinguishing between fast and slow diffusion to the Pt/Ru interface impossible in this work.

In this work, XANES and extended X-ray absorption fine structure (EXAFS) data were used to explore the surface reactivity and morphology of two ostensibly similar PtRu (1:1) electrocatalysts, as well as a Pt_3Ru electrocatalyst. The wide differences seen in the CO coverage and oxidation are highlighted and correlated with the size and degree of alloying of the PtRu clusters.

Experimental

Materials.— Three types of carbon supported Pt-based electrocatalysts were used for preparation of the anodes. 30% PtRu (1:1) was obtained from DeNora N.A. ETEK Division (Somerset, NJ) (hereafter referred to as PtRuE). Two compositions of PtRu electrocatalyst (1:1 and 3:1) were prepared using the Watanabe method,[52] hereafter referred to, respectively, as PtRuW and Pt_3RuW. The anode (working) electrodes were prepared in-house with a metal loading of $\sim$45 mg/cm^2 by a standard vacuum table paper making technique.[36] The metal loading was chosen based on absorption cross sections for Pt and Ru to ensure a step height of close to 1 for the X-ray absorption spectroscopy (XAS) measurements. The electrodes were soaked in 1 M $HClO_4$ for 48 h, followed by vacuum impregnation.

The sealed compression cell used to obtain in situ XAS data has been described in detail elsewhere.[61] The membrane electrode assembly (MEA) was made by sandwiching a Nafion 1135 (1100 MW, 3.5 mm thick) membrane between the prepared anode and a Grafoil (carbon/graphite foil) counter electrode. The electrolyte used in these experiments was 1 M $HClO_4$ with the addition of 0.3 M methanol. The reference electrode was a reversible hydrogen electrode (RHE).

X-ray absorption.— A compression cell was used to obtain in situ XAS data, as described above. An Eco Chemie Autolab PGSTAT-30 potentiostat/galvonostat was used for potential control of the electrodes for XAS experiments. X-ray absorption data were taken at the National Synchrotron Light Source (NSLS) at Brookhaven National Laboratory at beam line X-23A2 in transmission mode with a three detector setup. The NSLS storage ring operated at 2.8 GeV and a current between 120 and 350 mA. The three detectors collected incident (I_0), sample (I), and foil transmission data (I_{ref}); i.e., the electrochemical cell was placed between the first and second detector and a reference foil of the metal of interest was placed between the second and third detectors. The transmission data of the reference foil was used for alignment, as described later. The Si 111 crystal monochromator was detuned by 15% for the Pt edges and 10% for the ruthenium edge to exclude higher harmonics. Measurements were taken at the Pt L_3 and L_2 edges and at the Ru K edge. Measurements were taken at the following potentials: 0.0, 0.24, 0.40, 0.54, 0.70, and 0.40 V (returning). All potentials are with respect to RHE.

Computational Analysis

XANES analysis.— Analysis of the XANES (near-edge) region of the XAS data was carried out using the novel $\Delta\mu$ technique,[62-70] previously applied to adsorption of H, O, and OH on Pt[62,63] and Pt–M (M = Cr, Fe, Co, and Ni) cathodes[70] in an electrochemical cell, and even to Pt and PtRu anodes in an operating direct methanol fuel cell.[54] A brief summary is given here for clarity and to highlight slight differences from the previous method.

The absorption coefficient, μ, was obtained from the raw data using the ATHENA code of Ravel and Newville.[71] After linear combination of appropriate channels of the raw data, the pre-edge background was removed using the AUTOBK algorithm, described more fully elsewhere,[72] followed by normalization over the 20 to 150 eV (relative to the edge) range for XANES analysis. This procedure was carried out for both the sample data ($\ln I_0/I$) and the reference foil data ($\ln I/I_{ref}$). The foil data were then aligned with each other using a group-developed code, and the resultant energy differences were transferred to the sample data; i.e., the ΔE determined for the foil at x potential was added to the energy of the data at the same x potential. This energy calibration corrects for shifts due to photon beam drift, and other possible effects. This energy calibration is crucial for the success of the $\Delta\mu$ technique to ensure full cancellation of the

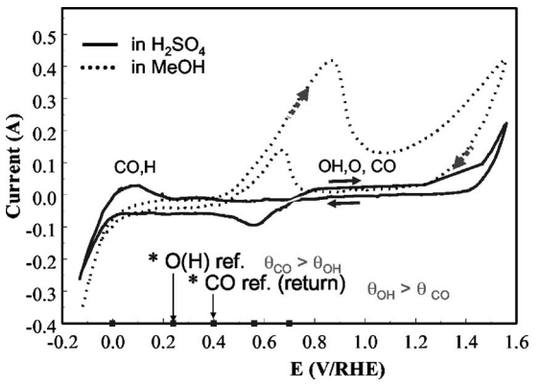

Figure 1. Typical CV curve for PtRu catalysts with and without methanol. The potentials where XANES data were taken are indicated by the small squares, and the references chosen for determining the $\Delta\mu$ for CO and O(H) isolation are indicated as described in the text.

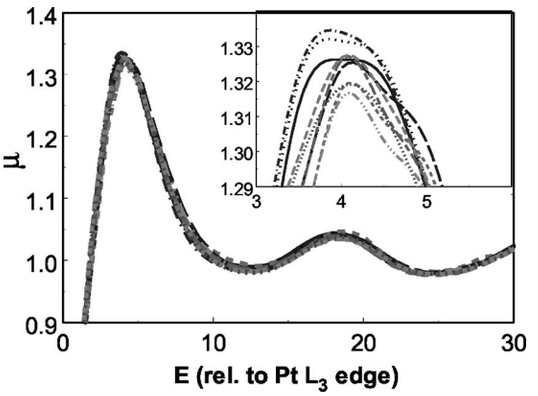

Figure 2. Pt L_3 edge XANES for PtRuE sample in 1 M $HClO_4$ or in 1 M $HClO_4$ plus 0.3 M MeOH at different potentials to illustrate the similarity yet systematic difference in the data.

atomic contribution in the XANES, which dominates the spectrum; i.e., $\Delta\mu$ is typically only about 1–5% of the total μ signal.

The difference $\Delta\mu = \mu(V) - \mu(V_{ref})$ is generally determined by subtracting the μ at an appropriate reference potential, V_{ref}, (usually taken to be at that potential when the electrode is relatively free of most adsorbates) from other potentials to highlight the effect of these adsorbates. To determine simultaneous relative concentrations of CO and O(H) at the Pt edge, a more complex method was necessary, because no potential in methanol exists when no CO, H, or O(H) is present as summarized in the typical CV curve in methanol (shown in Fig. 1). One could, of course, use as reference the electrode in the absence of methanol when no CO would be present, but we prefer not to for reasons given below. The best reference potential for determining CO concentration here is believed to be that in methanol at 0.40 V upon returning from higher potential (termed 0.40R below), as this is the potential at which the least amount of CO is present (some of the CO has been oxidized upon bringing the potential above 1 V RHE and only a modest amount of it has readsorbed upon returning to 0.40 V, as will be shown below). Therefore, the CO signal can be obtained from the difference

$$\Delta\mu(x,\mathrm{CO}) = \mu(x) - \mu(0.40\mathrm{R}) \qquad [3]$$

To extract the O(H) (i.e., O or OH) signal, the spectra taken at 0.24 V is used as the reference as illustrated in Fig. 1. A minimum of O(H) is present at 0.0 and 0.24 V; however, the spectrum at 0.0 V might include unwanted contributions from adsorbed H, so we use the 0.24 V spectrum. A scaled portion of $\Delta\mu(0.24,\mathrm{CO})$ from Eq. 3 is then added to remove the CO signal shown to be present at all lower potentials. The scale factor, a, is chosen to minimize $\Delta\mu$ in the positive energy region (~7.5 to 11 eV relative to Pt edge) where the CO contributes a large magnitude to $\Delta\mu$. Thus

$$\Delta\mu(x,\mathrm{OH}) = \mu(x) - \mu(0.24) + a\Delta\mu(0.24\ \mathrm{V,CO}) \qquad [4]$$

At the Ru edge, only one reference potential was used; however, it varied based on the electrocatalyst. The optimum V_{ref} was determined based on the continuity of species present as observed by taking step-wise differences (i.e., $\Delta\mu$ for consecutive potentials). For PtRuE, 0.40 V on the return was used, while for PtRuW 0.0 V was used as the reference. The Ru K edge data was not obtained for Pt_3RuW.

As shown in Fig. 2, the $\Delta\mu$ represents a small (1–2%) deviation form μ; however, the adsorbate $\Delta\mu$ signatures obtained vary systematically as shown below with the noise levels in $\Delta\mu$ less than 10% after applying a 3–5 point (~2 eV) smoothing function.

EXAFS analysis.— EXAFS analysis was carried out using the Athena and Artemis codes[71] from the IFEFFIT package.[73] The absorption coefficient, μ, was obtained from the Athena program in a manner identical to that described above for the XANES region, with the exception that the normalization range was changed from 150 to ~ 1600 eV relative to the Pt edge, and from 150 to ~ 1100 eV relative to the Ru edge. The deconvoluted data was then saved as $\chi(k)$ and imported into the Artemis program for fitting. A FEFF 8.0[74] calculation on a Pt_4Ru_2 "Janin cluster"[75] (Fig. 3 inset) was imported to model the Pt–Pt and Pt–Ru paths at the Pt edge, and a similar calculation was performed at the Ru edge using a Ru–Pt

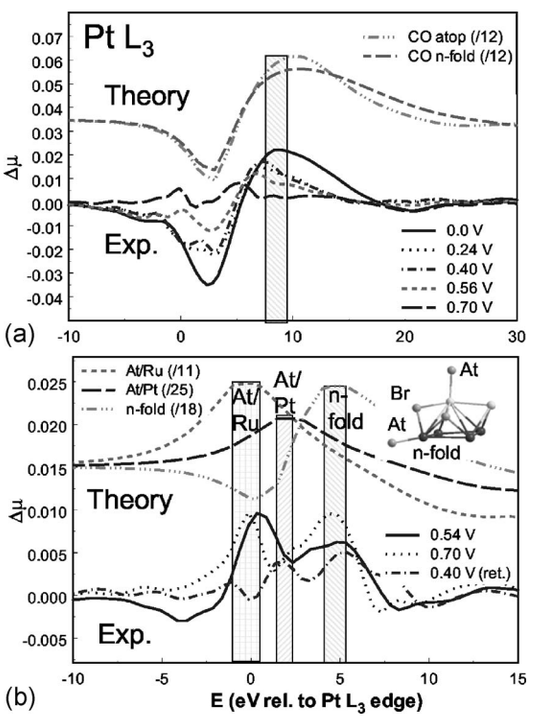

Figure 3. Pt L_3 edge $\Delta\mu$ spectra for PtRuW sample using 0.40 V on the return as the reference (a) or 0.24 V as the reference with a correction factor for CO as described in the text (b). Theoretical signals from FEFF 8.0 for CO adsorbed in atop and n-fold sites shifted up by 2.5 eV (top) and for OH atop and O n-fold shifted as described in the text are included with optimal alignment with experiment. The shaded areas indicate regions utilized to determine relative CO and O(H) coverages. A representative Pt_4Ru_2 Janin with O adsorbate in atop, bridged, and fcc (n-fold) positions is also shown.

path and a Ru–Ru path. For PtRuE and PtRuW, simultaneous fitting was carried out at both the Pt L_3 and Ru K edges.

The many-body S_0^2 factor calculated by FEFF 8.0, S_0^2 (FEFF), was 0.934 for the Pt edge and 0.916 for the Ru edge. Artemis calculates a factor called "amp" for each path, which should correspond to the experimental S_0^2, assuming the model cluster used in FEFF and the experimental cluster are exactly the same. This is not true in our case, as the model cluster is much smaller than the experimental cluster in general. However, using the path degeneracy for the nearest neighbor distance from the model cluster [this corresponds to N(model) for the cluster], we should have

$$S_0^2(\text{FEFF})/N(\text{model}) = \text{amp}/N(\text{exp}) \quad [5]$$

Therefore the experimental coordination number for each path, N(exp), may be determined as follows

$$N(\text{exp}) = \text{amp} * N(\text{model})/S_0^2(\text{FEFF}) \quad [6]$$

FEFF 8.0 calculations.— The FEFF 8.0 code was used to model adsorbate signatures in the XANES region, as well as to fit the EXAFS region. The $\Delta\mu$(Ads) was determined by subtracting the μ of the clean Janin cluster[75] from the μ of a cluster containing an adsorbate molecule in the atop, bridged or n-fold position (Fig. 3 inset); i.e., $\Delta\mu = \mu(O/Pt_4Ru_2) - \mu(Pt_4Ru_2)$. The Janin cluster, used in much but not all of our previous work,[62-70] was chosen here because it contains atop, bridged, fcc, and hcp sites, and the particular configuration was established to include Pt–Pt, Pt–Ru, and Ru–Ru paths for EXAFS analysis. The M–M (M = Pt,Ru) bond distances used in all FEFF 8.0 calculations was 2.75 Å, M–C = 1.85 Å, C–O = 1.0 Å, O–H = 1.0 Å, and M–O = 2.0 Å. Oxygen in the atop position was treated as OH (because the scattering from H is negligible), while oxygen in an n-fold position was treated as O. This is consistent with chemical intuition and density functional theory calculations,[63] which show that OH prefers to be singly coordinated, and O doubly or triply. In FEFF 8.0, a unique potential was calculated for each Pt, Ru, and O atom to allow for different surroundings of each atom.

Results

XANES analysis.— *CO signal*.— Figure 3a shows typical Pt L_3 edge $\Delta\mu$ spectra emphasizing the CO signal, compared with atop and n-fold signals for CO, calculated using FEFF 8.0. Note the narrowing of the theoretical CO peak around 8 eV for the atop CO compared to the bridged CO. The experimental $\Delta\mu$ shows this same narrowing upon going from 0.0 to 0.24 V and higher, consistent with the known conversion of some bridged CO to atop CO with decreasing CO coverage at higher potentials.[76,77] The height of each peak in the highlighted region was evaluated to determine the relative amounts of CO present at different potentials. Note further that the $\Delta\mu$ signature at 0.70 V does not reflect CO, but now O(H) in three different sites. Figure 4a shows experimental data with CO present, as well as the theoretical FEFF 8.0 calculations for CO atop and n-fold at the Ru K edge. There is little differentiation between CO in the atop and n-fold positions. The amplitude of the spectra in the CO region (10 to 15 eV) was measured to estimate relative CO concentrations at the various potentials. The change in spectral shape with increasing potential again reflects the change from CO coverage to O(H) coverage to be shown below.

O(H) signal.— Figure 3b again shows representative Pt L_3 edge $\Delta\mu$ spectra, in this case emphasizing the contribution of oxygen to the spectra, which was previously hidden by the negative portion of the CO peak in the −2 to 7 eV range. Three peaks are visible in the oxygen region, corresponding to (in increasing energy) OH atop "near" a Ru island, OH atop "away from" a Ru island, and O in an n-fold position. Due to the small size of the Janin cluster, it is not expected that a differentiation can be made between near and far from the Ru atoms in a FEFF 8.0 calculation on Pt_4Ru_2, as necessarily all atoms are "close" to each other. However, we can mimic

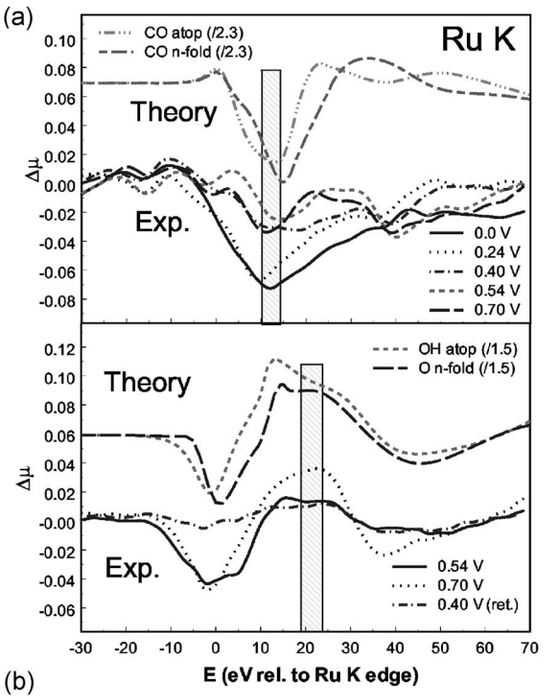

Figure 4. Ru K edge $\Delta\mu$ for PtRuE sample using 0.40 V on the return as the reference (a) and for PtRuW sample using 0.0 V as the reference (b), and theoretical FEFF 8.0 signals for CO and OH as indicated, the latter shifted up by 5 eV for optimal agreement with experiment.

the effect of the "away from Ru" atom by modeling O(H) on a Pt_6 Janin cluster. Although a single FEFF 8.0 calculation does not reproduce the three peak structure seen in the data, nor reproduce the full shift, FEFF 8.0 does predict twice the gap in energy between the atop and n-fold positions in the Pt_4Ru_2 cluster compared to the Pt_6 cluster. Figure 3 shows the FEFF 8.0 calculated individual $\Delta\mu$ signals in which the OH atop near Ru peak has been moved down to mimic the doubled energy gap between the atop and n-fold positions.

This shift in the position of the OH/Pt peak close to a metal atom at the surface (Cr, Fe, Co, Ni, and Ru) has been seen before in bimetallics when M atoms are at the surface but not when they are absent,[54,70] and is believed to arise in part from a core level shift of the Pt L_3 level near a metal atom due to some charge transfer to the nearby Pt (i.e., a ligand effect). Furthermore, XANES analysis of pure Pt samples does not include the lowest energy OH peak, giving further evidence that this peak is the result of the mixed metal morphology.[63] The height of each experimental peak in the indicated highlighted regions was used to determine the relative O(H) species concentrations at each potential.

Figure 4b depicts both FEFF 8.0 theory for O(H) atop and n-fold species, as well as representative PtRuW data, at the Ru K edge. There is little differentiation between atop and n-fold O(H) species. The height of the spectra in the highlighted oxygen region (~20 to 25 eV) was measured to correlate relative oxygen levels present.

Summary of results.— Figure 5 shows the relative change of each indicated species determined from the $\Delta\mu$ amplitudes in the shaded regions as shown above at both the Pt L_3 edge and Ru K edge of the PtRuE sample at various potentials. Note that in Fig. 5 no attempt was made to include any scale factors to indicate absolute adsorbate coverage, so the plots show only the relative change in adsorbate coverage during the CV cycling, and each adsorbate is on a different scale (conversion to absolute coverage estimates will be made below). CO is observed at both the Ru and Pt surfaces, with

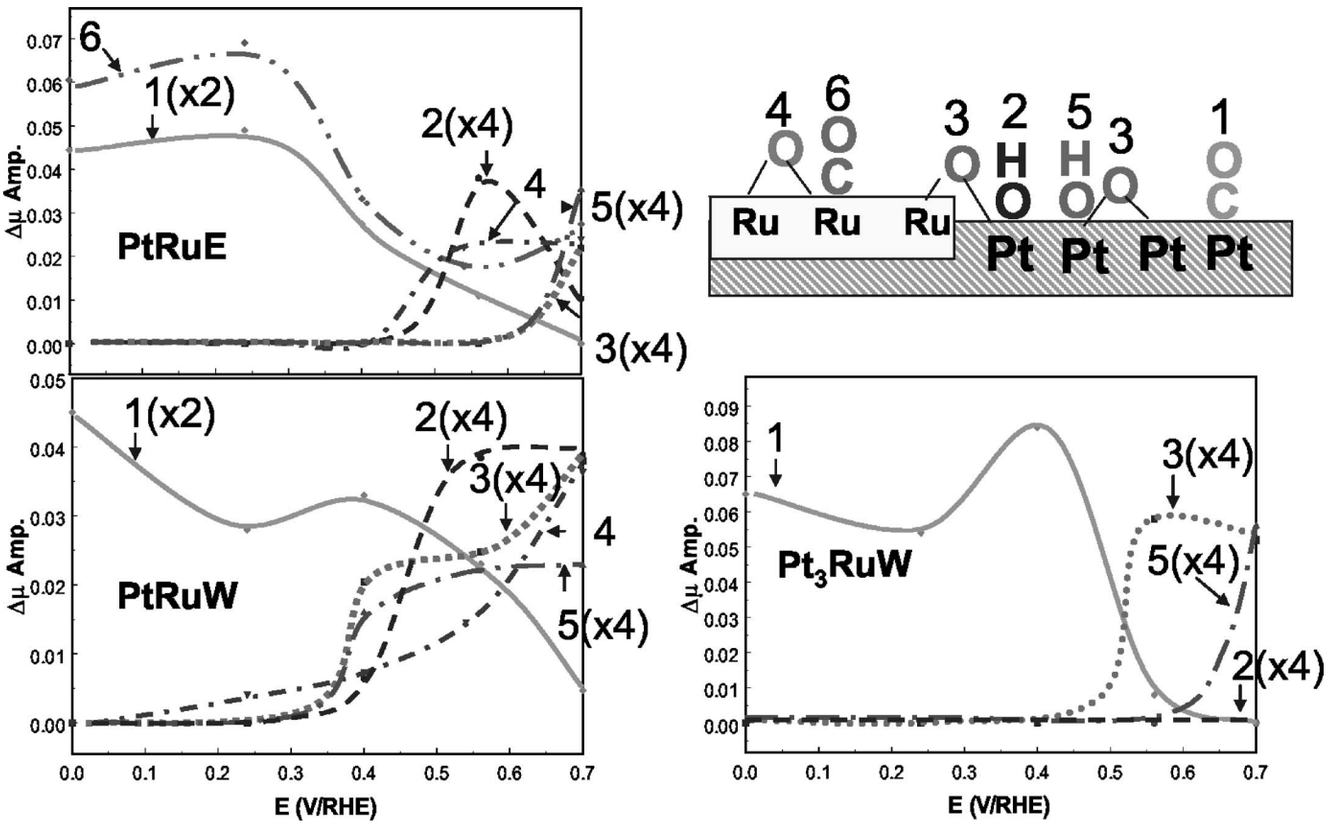

Figure 5. Δμ XANES amplitudes (obtained by the height of the shaded areas in Fig. 3 and 4) for the various adsorbates in the indicated catalysts with scale factors (*x* and *n*).

a higher amount at the Ru surface. The agreement between these results for CO and that reported previously by Freidrich et al.[57] using in situ IR data for Ru/Pt(111) is remarkable, except that the threshold for CO oxidation falls at 0.5 V in Friedrich instead of at 0.28 V as in Fig. 5. This is consistent with our discussion of Table I and the role of corners/edges in nanoparticles.

Figure 5 also shows the relative amount of each adsorbate present on the PtRuW sample at various potentials. The results are significantly different from the PtRuE case. No CO is present at the Ru edge, and that which is present at the Pt edge is removed in two distinct regions (from 0 to 0.25 V and from 0.45 to 0.7 V). Accumulation of oxygen on the Pt surface occurs earlier (beginning at 0.35 to 0.4 V) and occurs in the opposite order of the PtRuE case; that is atop OH/Pt "away from Ru" and *n*-fold O/Pt accumulate first, followed shortly by atop OH/Pt "near Ru."

Finally, Fig. 5 shows the relative concentrations of adsorbates on the Pt_3RuW. The pattern of adsorption is similar to that on PtRuW. There is again no CO evident (or at least change in CO coverage) on the Ru surface. The CO concentration on the Pt surface again is decreased in two distinct regions, 0 to 0.25 V and 0.4 to 0.6 V. The order of oxygen accumulation in this case is identical to that of PtRuW; that is, *n*-fold O/Pt begins to accumulate around 0.45 V, followed by atop OH/Pt "away from Ru" (around 0.65 V). Within the experimental range, atop OH/Pt "near Ru" is never seen to accumulate.

EXAFS analysis.— The EXAFS analyses of the three electrocatalysts at the Pt L_3 and Ru K edges are summarized in Table II. In all cases, the Debye-Waller factor σ^2 was held at 0.005 $Å^2$ to allow meaningful comparison of the coordination numbers, *N*, for all cases (the high correlation between *N* and σ^2 makes the change in *N* less meaningful when both are allowed to vary). Setting σ^2 to a series of values between 0.002 and 0.008 $Å^2$ confirms the strong linear dependence between *N* and σ^2. The optimum value was determined by fitting in k^1, k^2, and k^3 space at each of these σ^2 values and locating the intersection point following a procedure developed by Koningsberger et al.[78] Note further that $N_{Pt–Ru}$ and $R_{Pt–Ru}$ are the same at the Pt L_3 and Ru K edges, because these data were fit simultaneously, with single parameters for these quantities; i.e., the same "delr" and dependent, weighted "amps" as shown

$$\begin{aligned}&\text{amp(Pt edge)}\\&\quad = S_0^2(\text{Pt edge})/S_0^2(\text{Ru edge})^{*}\text{amp(Ru edge)}\\&\quad = 1.02\ *\ \text{amp(Ru edge)}\end{aligned} \qquad [7]$$

Thus, both the Pt L_3 and Ru K data were fit together with a total of 10 parameters each for PtRuE and PtRuW.

The magnitudes of N_{Total} at the Pt edge indicate particle sizes ranging from about 1.2 to 1.6 nm, on the basis of model cluster calculations assuming spherical clusters.[79] Although it is not claimed that these are perfectly spherical clusters, this does illustrate the difference in size and dispersion (0.7 to 0.88) for these clusters. Note the decreasing $R_{Pt–Pt}$ and $R_{Pt–Ru}$ with decreasing cluster size (PtRuE and PtRuW), consistent with that found previously (For example, see, for example, Ref. 80), and attributed to decreased bond length with decreasing atom coordination. Note also the much larger bond lengths in Pt_3RuW, consistent with the larger fraction of Pt present in the cluster. Much less Ru is present in the Pt_3RuW case to shrink the lattice.

Figure 6 shows a comparison of the Fourier transforms of the EXAFS data (*k*: 2 to 15 $Å^{-1}$,k^1) for the three electrocatalysts studied here and a 20% Pt/C electrode, all at 0.04 V RHE in 1 M $HClO_4$. In the 2.5 Å region, the well-known region of highly de-

Table II. Summary of in situ EXAFS results from Pt L_3 edge at 0.58 V RHE and Ru K edge at 0.04 V RHE and comparison with model results.

Electrocatalyst	N_{Pt-Pt}	R_{Pt-Pt} (Å)	σ^2 (Å^2)	E_0 (eV)	N_{Pt-Ru}	R_{Pt-Ru} (Å)	σ^2 (Å^2)	E_0 (eV)	N_{Total}	N_{Pt-Ru}/N_{Pt-Pt}
PtRuE	6.10	2.74	0.005	0.3005	2.54	2.72	0.005	1.621	8.64	0.416
PtRuW	4.38	2.73	0.005	−2.258	2.82	2.71	0.005	1.985	7.20	0.644
Pt_3RuW	7.53	2.76	0.005	−0.071	0.75	2.79	0.005	9.250	8.28	0.100
	N_{Ru-Ru}	R_{Ru-Ru} (Å)	σ^2 (Å^2)	E_0 (eV)	N_{Ru-Pt}	R_{Ru-Pt} (Å)	σ^2 (Å^2)	E_0 (eV)	N_{Total}	N_{Ru-Pt}/N_{Ru-Ru}
PtRuE	2.58	2.66	0.005	−11.22	2.54	2.72	0.005	−14.21	5.12	0.984
PtRuW	2.92	2.66	0.005	−2.220	2.82	2.71	0.005	−8.507	5.74	0.966
Model	N_{Pt-Pt}	N_{Pt-Ru}	N_{Pt-Ru}/N_{Pt-Pt}	N_{Total}	N_{Ru-Pt}	N_{Ru-Ru}	N_{Ru-Pt}/N_{Ru-Ru}	N_{Total}		
PtRuE	6.10	2.66	0.436	8.76	2.66	2.65	1.00	5.31		
PtRuW	4.36	2.82	0.647	7.18	2.82	2.92	0.966	5.74		
Pt_3RuW	7.53	0.76	0.101	8.29						

structive interference between Pt–Pt and Pt–Ru scattering is apparent, demonstrating some level of alloying in the PtRu(1:1) samples, and showing that in Pt_3Ru, a large excess of Pt–Pt scattering is present (i.e., nonalloyed regions).

Figure 6 also reveals the goodness of fit of the EXAFS analyses. For the case of the PtRuE sample, it compares the magnitude of the Fourier transforms of the data, fit, and separate Pt–Pt and Pt–Ru paths. Note again the destructive interaction at 2.5 Å.

Discussion

Cluster morphology.— To understand the large differences seen in the adsorbate coverages for these samples as revealed in Fig. 5, appropriate models were developed for the structure or morphology of the average PtRu cluster in each sample based on the EXAFS results, using the Atoms code[71] to generate different cluster models.

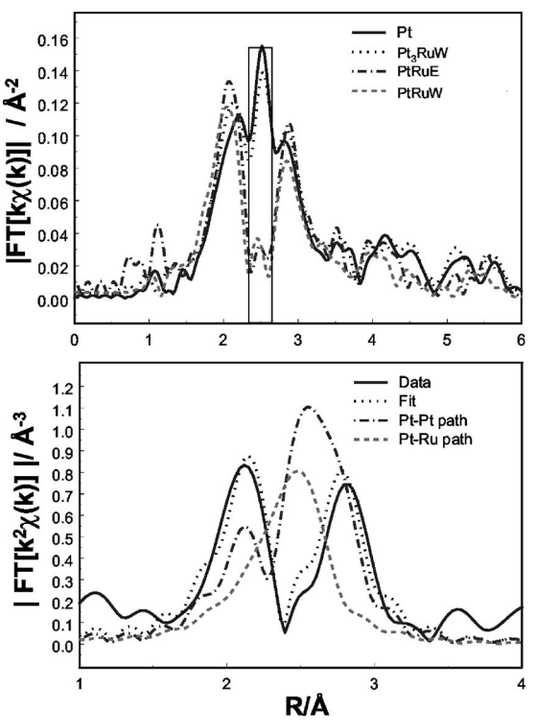

Figure 6. Magnitude of FT for Pt and PtRu samples, showing destructive interaction of Ru and representative fit for PtRuE sample with indicated paths.

The nearest neighbor coordination of each atom divided by the total number of atoms of that type then gives the average coordination number. We assumed oxidized Ru removed Ru–Ru scattering because the presence of an O atom between the Ru atoms or even in its close proximity is known to strongly reduce the metal-metal scattering;[63,81] thus oxidized Ru atoms had zero Ru–Ru coordination. Recall that at least for the 1:1 alloys, we have three coordination numbers to suggest something about the morphology of the clusters. The optimal models are shown in Fig. 7 and their relative coordination numbers in Table II. Comparing the model and experimental results in Table II, one can see that less than 5% deviation exists between the model and the experimental data in the case of the PtRuE model, and the other two models correlate to within 0.5%.

One can legitimately question the uniqueness of the optimal models shown in Fig. 7. Figure 8 attempts to illustrate how sensitive the coordination numbers are to the different assumed Pt and Ru morphologies by showing a number of models considered for both the PtRuW and PtRuE samples. The upper shaded band in Fig. 8 represents a ±5% deviation from the calculated N_{Pt-Pt}, while for clarity, the lower shaded band encompasses the same window for both $N_{Pt-Ru/Ru-Pt}$ and N_{Ru-Ru}. The models marked A represent highly segregated configurations; essentially a small Pt particle joined to a small Ru particle. Models marked B, by contrast, correspond to extremely well-alloyed morphologies. Models marked C contain a higher order Pt core (Pt_nRu where $n > 1$) with a Ru skin of various depths. Finally, models marked D are those deemed acceptable; the only models discovered for which all three coordination numbers fall in or near the acceptable windows. As can be seen, many models may accurately reproduce two coordination numbers, but few can accurately model all three.

In Fig. 8, for PtRuW, the models depicted range in size from 28 to 44 atoms. The only two models that closely reproduce the three calculated coordination numbers are 8 and 11. Model 11 not only

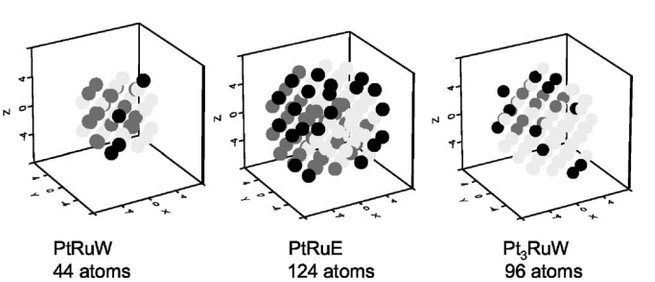

Figure 7. Model for indicated electrocatalyts: white Pt, gray Ru, black $Ru(O)_x$.

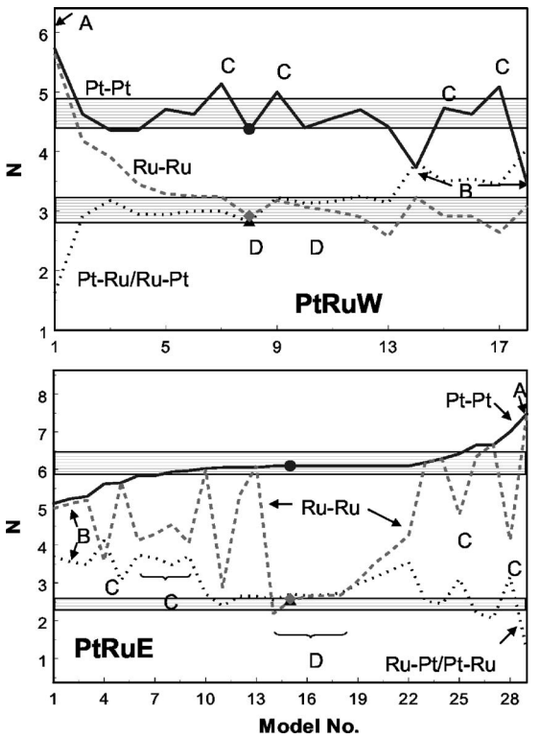

Figure 8. Various models for PtRuW (top) and PtRuE (bottom). Shaded areas represent ±5% deviation from experimental EXAFS fits. For clarity, the lower error bar encompasses both Ru–Ru and Pt–Ru/Ru–Pt.

falls farther from the acceptable window, but also is substantially smaller (30 atoms) than model 8 and contains no oxidized Ru atoms, which is not believed to be reasonable. Model 8 represents the configuration shown in Fig. 7. This model contains 44 atoms, arranged in a reasonably well-alloyed configuration, with 4 $Ru(O)_x$ islands at the surface. Based on the dispersion[82] for a cluster of this size, all but 5 atoms are at the surface, and only 20% of the surface Ru atoms are oxidized.

The PtRuE model is quite different, both in size and configuration. Of the 29 models shown in Fig. 8, models 14 through 18 most closely approximate the values in Table II. Of these, models 14, 15, 16, and 18 are identical except for the degree of oxidation, and model 17 is only slightly different. All contain around 120 atoms, with a Pt_2Ru core comprising ~60 atoms, a somewhat segregated PtRu layer of around 40 atoms, and a Ru "skin" of around 20 atoms. The best fit is obtained by model 16, which consists of a Pt_2Ru core of 63 atoms, a somewhat segregated PtRu layer of 40 atoms, and a Ru "skin" of 21 atoms. The entire Ru skin is oxidized in model 16, one-third of the total Ru atoms present. The larger cluster has only 70% of its atoms at the surface, and about 40% of the Ru atoms, those at the surface, are oxidized.

The Pt_3RuW model contains 96 atoms, with a somewhat segregated configuration. The core of the model is 90% Pt, with the remainder of the Pt atoms distributed in a Pt_3Ru configuration. Conversely, the outer 20 atoms are only 60% Pt. The outer eleven Ru atoms are oxidized, which corresponds to approximately half of the Ru atoms.

Based on these optimal models, which of course should be regarded as average and representative only, one can briefly characterize the difference between the three electrocatalysts under the conditions existing in the cell corresponding to nonadsorption (0.58 V for Pt L_3 edge, 0.04 V for Ru K edge in 1 M $HClO_4$). The PtRuE clusters are relatively large with the Ru and Pt atoms poorly mixed and the Ru oxidized on the surface. The PtRuW clusters are much smaller with the Pt and Ru more evenly mixed (alloyed), the Ru atoms more monodispersed, and relatively less of the Ru oxidized at the surface. Finally, the Pt_3RuW clusters are intermediate in size with the Ru more alloyed. However, the much larger Pt:Ru ratio leaves large components of pure Pt, and a considerable amount of Ru oxidized at the surface. These qualitatively different morphologies help to explain the different CO oxidation regimes found from the XANES data.

Converting $\Delta\mu$ magnitudes to absolute coverage.— Figure 5 plots the $\Delta\mu$ amplitudes in the highlighted regions of Fig. 3 and 4. The scale factors (SF) applied to the theoretically calculated $\Delta\mu$ signatures in Fig. 3 for CO and O(H) at the Pt L_3 edge and in Fig. 4 for CO and O(H) at the Ru K edge, were determined to provide comparable magnitudes with the experimental data. Because the Janin cluster (Fig. 3 inset) used for the FEFF 8.0 calculation has a Pt absorber atom-adsorbate atom coordination number of 1 (i.e., the photon absorber atom is always placed next to the adsorbate), these scale factors give a reasonable measure of the coverage change from the reference ($\Delta\theta$) in units of ML adsorbate per total absorber atom (M_{tot}); i.e., $\Delta\theta(ML/M_{tot}) = \Delta\mu_{exp} * SF/N_c$ with N_c to be discussed below. This coverage change is relative to M_{tot}, because the XAS spectra are normalized to one, and the XAS samples all atoms present in the beam cross-sectional area. After making some assumptions about the dispersion of the Pt clusters and the fraction of accessible Pt and Ru sites relative to the total, one can make some estimates of the coverage per geometrically accessible surface atom $[\Delta\theta(ML/M_{acc})]$ or active site; i.e., assuming the relative number of active sites is $M_{acc} = M_{tot} * D * F_{cont} * F_{cov}$, where D is the dispersion factor, $D = M_{surf}/M_{tot}$ of about 0.7–0.9 based on the cluster sizes found,[79] F_{cont} accounts for cluster contact (i.e., M-carbon support and cluster-cluster contact making these sites geometrically unavailable for CO or O(H) adsorption), and F_{cov} accounts for coverage of Pt by the Ru islands with the generally Pt-rich core and Ru-rich shell structure found for small Pt–Ru particles.[83]

Although estimates of the relative coverage may be only semiquantitatively correct, due to unknowns about the amount of accessible Pt surface sites, etc., such estimates can still be very helpful in understanding the extent of adsorbate coverage and help us to understand the relative activity of the different mechanisms.

It should be emphasized that the experimental μ is proportional to the metal-adsorbate coordination number, N_c, and therefore $\Delta\theta$ obtained from $\Delta\mu$ should take this factor into account as included above. For example, CO can exist in the three-fold, bridged or linear (also called atop) sites, with the distribution among sites generally changing with coverage. For CO/Pt(111) in a (2×2)-3CO unit cell at a maximum coverage of 0.75 ML,[76] 1 CO is in an atop site and two- in threefold sites spread over 4 Pt atoms. The average Pt–CO coordination number is then $(1 * 1 + 3 * 2)/4 = 7/4$ or put another way, the average Pt atom "sees" 1.75 CO molecules at maximum coverage on Pt(111). Therefore, although the $\Delta\mu$ signatures and magnitudes, as shown in Fig. 3, are nearly the same for atop CO and n-fold CO when one CO is placed next to a Pt absorber atom, the magnitudes of $\Delta\mu$ at full coverage will depend on the site; i.e., a factor of 3 bigger for a full ML of threefold CO vs a full ML of atop CO. As the coverage decreases, this factor may decrease or stay the same depending on the change in unit cell structure; e.g., the CO goes to a $\sqrt{19} \times \sqrt{19}$ unit cell structure at 0.687 ML with N_c still around 1.7, and eventually is expected to decrease to 1 when a very diffuse adlayer exists on Pt(111).[76] For small Pt particles with many corners and edges, the N_c factor is expected to be well below 1.7 even at maximum coverage because a greater fraction of atop CO is expected at these sites. Further, for OH/Pt, only atop sites are occupied, and the coverage of bridged O (when N_c might approach 2 at full coverage) is nearly always <0.5 in the potential regions considered here. Therefore, we shall ignore the N_c factor in all cases here, but the reader should recognize that it could be important for full CO coverage on big particles.

After applying the scale factors, SF, as indicated in Fig. 3 and 4 to provide optimum agreement between the theoretical FEFF 8.0 and experimental $\Delta\mu$ signatures, we obtain the maximum change in coverage (ML/Pt_{tot}) as follows

$$\Delta\theta_{CO/pt}(0.0V - 0.4RV\ RHE) = 0.08 \pm 0.01\ ML/Pt_{tot} \quad [8]$$

$$\Delta\theta_{OH/pt}(0.7V - 0.24V) \approx \theta_{OH/Pt}(0.7V) = 0.18 \pm 0.03\ ML/Pt_{tot} \quad [9]$$

where $\Delta\theta_{OH/Pt}$ consists of approximately $0.09 \pm 0.01\ ML/Pt_{tot}$ atop OH near Ru, $0.04 \pm 0.01\ ML/Pt_{tot}$ atop OH away from Ru, and $0.05 \pm 0.01\ ML/Pt_{tot}$ *n*-fold O. As is clearly evident from Fig. 4, the corresponding change in coverage (ML/Ru_{tot}) on the Ru atoms is much larger

$$\Delta\theta_{CO/Ru}(0.0V - 0.4RV) \approx \theta_{CO/Ru}(0.0V) = 0.43 \pm 0.05\ ML/Ru_{tot} \quad [10]$$

$$\Delta\theta_{OH/Ru}(0.7V - 0.24V) = 0.7 \pm 0.1\ ML/Ru_{tot} \quad [11]$$

where Eq. 8-11 assume that the O(H) coverage reflected in the reference spectra were near zero for this analysis.

Estimates of $\Delta\theta(ML/M_{acc})$ require estimates of several other factors as noted above. We assume that at 0.7 V, the coverage of O(H) species on Ru is around 1, thereby setting $F_{cont} = 0.6$ and, of course, $F_{cov} = 1$ here for Ru, assuming no surface Ru covered by Pt. The F_{cont} factor can be $\leqslant 0.7$ as found recently by Marković et al.,[84] when using a Pt loading on Vulcan carbon of 0.1 mg/cm^2. They obtained this value assuming that small Pt particles have the same HOR rate per surface Pt atom as bulk Pt(110), which may not be necessarily valid,[85] but it does give a rough estimate of F_{cont} similar to the result above. With $F_{cont} = 0.6$ then, this suggests a maximum change in CO coverage of around $\Delta\theta_{CO/Ru} = (0.43 \pm 0.05)/0.6 = 0.7 \pm 0.1\ ML/Ru_{acc}$ and of course $\theta_{OH/Ru} = (0.7 \pm 0.1)/0.6 = 1.2 \pm 0.2\ ML/Ru_{acc}$ or about 1 ML to within experimental uncertainty.

Some estimate of the factor F_{cov} for Pt [or at least the ratio $F_{cov}(PtRuW)/F_{cov}(Pt_3RuW)$] for the Pt surface can be obtained by comparison of the $\Delta\mu$ amplitudes in Fig. 5 near 0.0 V for the CO coverage [i.e., $\theta_{CO/Pt}(PtRuW)/\theta_{CO/Pt}(Pt_3RuW)$], which differ by a ratio of about 0.7. Assuming similar distribution of the Pt and Ru islands in the two Watanabe samples, and similar full CO coverage on both, one might expect this ratio to be 0.5. The experimental value of 0.7, a little larger than 0.5, is reasonably consistent with the cluster morphologies we found from the EXAFS models, which show Ru preferentially near the surface compared to Pt, and the general assessment that Ru islands of some sort exist on the Pt clusters. Assuming again that the coverage of all O(H) species is about $1\ ML/M_{acc}$ at 0.7 V, this suggests that $F_{cov}{*}F_{cont} = 0.15 \pm 0.01$ for the PtRuW sample (and we assume also for the PtRuE sample) and $F_{cov}{*}F_{cont} = 0.21 \pm 0.01$ for the Pt_3RuW sample, consistent with the ratio above. Assuming "full" CO coverage of $\theta_{CO/Pt}$ at 0.0 V is around $0.75\ ML/Pt_{acc}$ (consistent with the discussion above on Pt(111)) and $\theta_{CO/Ru}$ also around $0.75\ ML/Ru_{acc}$,[26] gives the coverage at 0.40 V on the return of about $0.75 - (0.08 \pm .01)/(0.15 \pm .01) = 0.2 \pm 0.06\ ML/Pt_{acc}$ for the PtRu 1:1 catalysts. Thus, our reference choice in methanol is proved to be a reasonably good one. On the other hand, the coverage of CO/Ru at 0.40 V on the return is near zero, $0.75 - (0.7 \pm 0.1)$ as expected.

The estimated coverages of $\theta_{CO/Pt} = 0.75$ and $0.2 \pm 0.06\ ML/Pt_{acc}$ at 0.0 V and 0.40 V on the return, respectively, can be tested by using a reference μ spectrum from a "clean" electrode; namely, a similar electrode in 1 M $HClO_4$ when the CO coverage should be zero. The ratio $[\theta_{CO/Pt}(0.0\ V) - \text{clean}]/[\theta_{CO}/Pt(0.0\ V) - \theta_{CO/Pt}(0.4R)] = 1.2 \pm 0.2$ is consistent with that expected $0.75/(0.55 \pm 0.06) = 1.4 \pm 0.2$ from the above analysis and lends support to our assumptions. This clean reference in 1 M $HClO_4$ was not used for all of the data analysis because in fact the PtRu clusters in 1 M $HClO_4$ and in CH_3OH were not exactly the same, leaving some Pt–Pt EXAFS contributions in the $\Delta\mu$ difference spectra, which interfered with our analysis. Nevertheless, they were sufficiently small to allow this test. Therefore, we conclude that our estimated coverage per "accessible" Pt and Ru atoms are semiquantitatively correct (with errors of around 10–20%) and the assumptions made to arrive at them are reasonable.

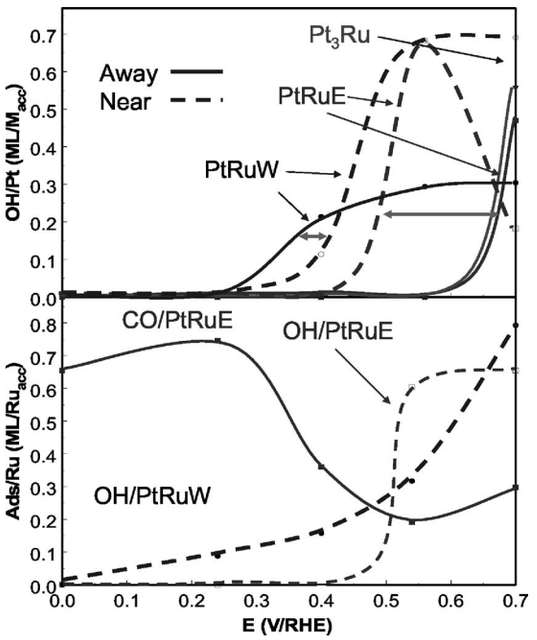

Figure 9. Estimated adsorbate coverages determined from the $\Delta\mu$ intensities and the assumptions summarized in the text for OH near and away from Ru islands (top) and that on the Ru (bottom).

Effect of morphology on the dominant mechanism.— Figure 9 compares the estimated coverages ($\Delta\theta$ in ML/M_{acc}) of OH/Pt near and separated (away) from the Ru islands (top) as well as O(H) and CO directly on the Ru (bottom). These comparisons reveal some interesting observations:

1. The coverage of OH/Pt away from the Ru islands for the smaller PtRuW sample appears nearly 200 mV below that for the larger PtRuE and Pt_3RuW samples. This is reasonably consistent with the 130 mV shift found recently by Marković et al.,[86] when comparing 1 and 30 nm clusters of Pt. It arises from the lower Pt–Pt coordination in the smaller clusters, making the Pt atoms more oxophilic.
2. The onset for OH/Pt near the Ru islands is shifted down from that for OH/Pt away from the Ru islands in the PtRuE sample by 250 mV. This is due to the well-known "ligand" effect of the Ru islands on the nearby Pt. Note however, a similar shift in the onset is not seen for the PtRuW sample. We believe two aspects contribute to this lack of a shift in the onset. First, the smaller size of the PtRuW clusters already makes the Pt atoms more oxophilic, and second, the more monodispersed Ru islands make them less effective as a ligand. This is discussed further below.
3. The onset for O(H) directly on the Ru islands is shifted down significantly in the PtRuW sample compared to the PtRuE. Furthermore, the PtRuE sample exhibits considerable CO directly on the Ru, while a similar coverage of CO/Ru in the PtRuW sample is not visible. Recall that the EXAFS analysis also showed that a significant portion of the Ru was oxidized at the surface of the PtRuE sample. This suggests strongly that the Ru islands on the PtRuE sample are highly reactive; so that they are covered with CO and O

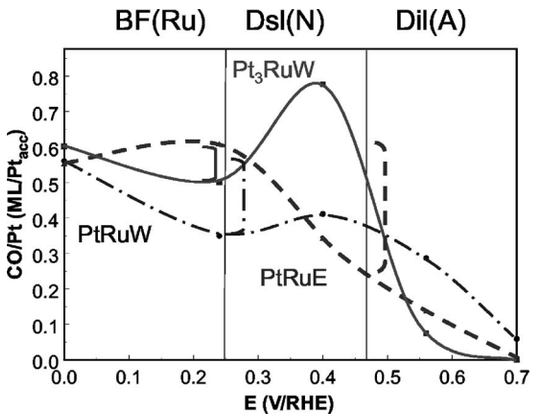

Figure 10. Estimated CO/Pt coverages determined as described in the text, and the indicated regions where each mechanism outlined in Table I is functioning. The brackets indicate the net amount of CO stripped via either the BF or Dsl mechanism due to mobile CO moving toward the Ru islands.

at low potential, and the OH necessary to carry out CO oxidation cannot come onto the Ru until some CO is removed. In contrast, the Ru islands in the PtRuW sample are apparently less reactive, allowing OH to adsorb at low potentials.

4. Figure 10 shows the CO coverage and the different regions where the CO is stripped from the Pt surface. It clearly shows the different potential regions where the CO is stripped and the dominant mechanism as summarized in Table I. Both Watanabe samples exhibit a significant BF stripping component below 0.3 V, consistent with OH coming onto the Pt surface in this region. However, this fractional component is larger in the PtRuW case than in the Pt_3RuW case as indicated by the brackets in Fig. 10. This is consistent with the larger fraction of Ru in the former case, so that more CO/Pt is in the vicinity of the Ru islands.

5. Figure 10 shows in contrast that the PtRuE sample exhibits a large Dsl component and no BF component. This is consistent with the onset for OH/Pt near Ru slightly earlier than that for OH/Ru as shown in Fig. 9. Furthermore, both the BF and Dsl mechanisms require mobile CO to move toward the Ru islands. We attribute the larger Dsl component to the larger Pt particles, and hence larger fraction of Pt(111) faces on these particles where the CO is mobile. We believe the CO is not sufficiently mobile on the edges/corners of the cluster, requiring the OH to come to the CO at these sites, i.e., requiring the Dil mechanism.

The oxidation state of the Ru islands.— What can cause this significant difference between actions of the Ru islands in the Watanabe vs E-TEK samples? We believe this arises from the size of the Ru islands. The Ru islands are apparently more monodispersed in the Watanabe samples, so that a "reverse" ligand effect from the Pt makes these Ru islands only slightly more reactive than the Pt, and therefore allows OH to come onto the Ru islands below 0.3 V RHE, but does not cause the Ru islands to be heavily oxidized at very low potential. In contrast, the proposed bigger islands in the PtRuE sample are much more reactive, therefore more oxidized already at low potential as exhibited by the EXAFS data and our models in Fig. 7, and further indicated by even adsorbed CO/Ru below 0.4 V. This high coverage of CO and inactive O on Ru below 0.4 V does not allow more OH to come on until some of the CO is stripped above 0.4 V. However, it appears that the larger and partially oxidized Ru islands in the PtRuE sample produce a more significant surface ligand effect on the Pt, making the Dsl component large in this case. It therefore appears that a reverse ligand effect of the Pt on the small monodispersed Ru islands is important in the Watanabe samples; however, a significant Ru ligand effect by the larger and partially oxidized Ru islands on the Pt is more important in the PtRuE sample.

This interplay between Pt and Ru, apparently determined (at least in part) by the relative size of the Ru islands and Pt particles as suggested here, has been discussed previously. For example, DFT calculations by Koper et al.[11] and by Desai and Neurock[87] show a weakening of the CO–Pt bond with addition of Ru and strengthening of the CO–Ru bond with addition of Pt, pointing to this interplay. Further, Lu and Masel[15] have shown that Ru/Pt has very different properties than Ru metal.

In the literature, there has not been total agreement on which phase of Ru is the most active for the complete oxidation of methanol to CO_2. For example, it has been suggested that catalysts consisting of two phases, namely Pt and hydrous Ru oxide (RuO_xH_y) are more active than PtRu alloy catalysts, i.e., Pt_0Ru_0.[88] In contrast, X-ray photoelectron spectroscopy (XPS) measurements carried out on Ru nanoparticles deposited on Pt(111) that involved the immediate transfer of the electrodes to a UHV chamber, suggested that the presence of a metallic Ru phase, which is covered by a weakly bonded Ru oxidation state precursor like Ru–OH, is a prerequisite for the BF mechanism.[89] Furthermore, recent studies show that the kinetics of CO oxidation are slower for catalyst-containing Ru-oxides as opposed to mainly Ru metal.[90]

In situ XANES measurements performed on PtRu catalysts in methanol also produced conflicting conclusions as to the Ru oxidation state. Smotkin's group[55] indicated that, within the direct methanol fuel cell (DMFC) operating potential window (250 to 450 mV vs H_2 reference electrode), the relatively large near neighbor oxygen atoms per Ru atom ratio is insensitive to potential, as suggested by the lack of significant changes in the Pt or Ru edge XANES data. However, Roth et al.[54] show that the Ru, although oxidized in air, become reduced immediately upon exposure to methanol or hydrogen. These widely different conclusions could arise from possibly different PtRu cluster morphologies utilized in the two XAS studies, but more probably arise from different interpretations of the XANES data. Roth et al.[54] utilized the $\Delta\mu$ technique, as employed in this work, which examines small changes in the XANES spectra. As shown above, just 1–3% changes in the XANES can indicate large changes in the O(H) coverage, so that perhaps the small XANES changes observed by Smotkin's group do not necessarily indicate little reduction of the Ru.

More consistent with Roth's conclusions above are in situ current-time transient measurements done in methanol in such a way as to allow separation of the double-layer charging current (the oxidation of methanol, and the oxidation of Ru). They suggest that the presence of methanol decreases the amount of reversibly reducible Ru oxides.[91] Bock et al. also examined the methanol oxidation activity as a function of electrochemically preformed vs not preformed Ru-oxides. These experiments were carried out at constant potentials of 0.4, 0.6, and 0.8 V for a PtRu alloy catalyst. It was confirmed that the presence of electrochemically preformed Ru-oxides lowered the methanol oxidation activity; however, the catalytic de-enhancing effect is only observed at potentials higher than 0.6 V. Furthermore, the decrease in the methanol oxidation activity was in the low percentage range (ca. 5 and 15% at 0.6 and 0.8 V, respectively). These results suggest that even preformed Ru oxides are either reduced or have little effect in the typical DMFC operating window. These results are also consistent with previously reported in situ ellipsometric studies.[92] Thus, the overwhelming evidence is that Ru in PtRu bimetallic clusters must be reduced to some extent to be an effective catalyst, and that in general some or all of the Ru is indeed in this state.

However, this still leaves open the question of how the Ru island size and Pt morphology affect the oxidation level, and thus, catalytic behavior. The in situ current-time transient studies reported by Bock et al.[91] suggest that the Ru in well-distributed Pt to Ru surface sites in methanol concentrations greater than 0.5 M, remains in the reduced, metallic state during the methanol oxidation reaction. In the

Pt/Ru catalyst surfaces composed of poorly distributed Pt to Ru surface sites, the presence of methanol suppresses Ru-oxide formation; however, Ru-oxides are found to form to some degree. These latter conclusions by Bock et al.[91] are consistent with the conclusions found in this work regarding the importance of the Ru island size and morphology, and that indeed, poorly distributed Pt to Ru surface sites, with presumably larger Ru island size, are partially oxidized even in methanol.

Other studies of the structural effects and reactivity for methanol oxidation have also been reported previously. For example, Vielstich's group used in situ Fourier tranform infrared (FTIR) as well as other electrochemical techniques to study CO adsorption in methanol with different PtRu morphologies.[93-96] They concluded that "more porous" PtRu surfaces showed the least current decrease during chronoamperometric experiments, consistent with smaller Ru islands and the apparent increased effectiveness of the BF mechanism. Likewise, the Adzic group studied varying amounts of Pt coverage on Ru nanoparticles in H_2 with trace amounts of CO. $PtRu_n$ (with $n = 20$, 10, and 5) were studied and found that the percentage of blocked Pt sites after full exposure did not change significantly with n. They therefore concluded that the limited CO tolerance is not due to the limited amount of Ru sites, but to the strong CO adsorption on Ru, poisoning these sites.[97-99] In light of our work, we suggest that the majority of Ru sites (comparable to the big Ru islands in this work) are highly active and hence get covered by CO, but those in the periphery of the Pt particles, where a reverse ligand effect from the Pt is present, adsorb OH, allowing the BF mechanism to function.

Finally, many reports of low PtRu loadings and different heat-treatments showed superior CO-tolerance levels.[6,8] Heat-treatment at 600°C in vacuum or argon atmosphere was found to increase the PtRu particle size, reduce the amount of Pt on the nanoparticle surface, and thereby increase the surface Ru content. This caused a large reduction in methanol oxidation activity. On the other hand, heating at 220°C in H_2 led to a threefold increase in methanol oxidation per surface site.[100] These studies, in light of work here, again point to the importance of metallic Ru at the surface, but in limited or dispersed amounts, else it becomes covered with CO and/or oxidized even in methanol, shutting off the BF mechanism. Finally, Bock et al.[101] suggest that 1 Ru and 3 neighboring Pt sites is ideal for CH_3OH oxidation, as suggested by the relative activities of a wide range of PtRu alloys when the bulk and surface compositions are similar; i.e., the particles are well alloyed.

Although supported by the previous work summarized above, to our knowledge the results reported in this paper provide the first direct spectroscopic evidence for the critical importance of the Ru island size in determining the overall dominant mechanism (BF vs Dsl) for CO stripping at a PtRu electrode; namely, that the BF dominates for small Ru islands, and the Dsl for bigger Ru islands, when the Ru is partially oxidized.

Conclusions

The activity of CO and O(H) on three different PtRu electrocatalysts was found to depend strongly on the cluster size and morphology. While the basic CO oxidation mechanisms remain the same, their relative effectiveness changes. Both the bifunctional mechanism involving OH formation on the Ru islands, and the direct mechanism involving OH formation directly on the Pt but enabled by the electronic effect are active, but the relative importance of these mechanisms depends critically on the morphology and size of the particles, as summarized in Table I. Both the particle size and, more importantly, the Ru island size, are critical to determining the relative magnitude of the different mechanisms.

This work suggests that one can tune one of the three mechanisms to dominate by changing the particle morphology and size. Further, because the bifunctional mechanism and the two different direct mechanisms dominate at different potentials, this data suggests that the particle morphology determines whether a catalyst will be operative optimally in reformate or in methanol, as the anode is generally at lower potential in reformate, when the bifunctional mechanism is operative, and higher potential in methanol, when the direct mechanisms are operative. Further work on this will be reported in a forthcoming publication.[102]

References

1. N. M. Marković and P. N. Ross, *Surf. Sci. Rep.*, **45**, 117 (2002).
2. J. Kua and W. A. Goddard, III, *J. Am. Chem. Soc.*, **121**, 10928 (1999).
3. M. C. Denis, P. Gouerec, D. Guay, J. P. Dodelet, G. Lalande, and R. Schulz, *J. Appl. Electrochem.*, **30**, 1243 (2000).
4. Y. Tong, H. S. Kim, P. K. Babu, P. Waszczuk, A. Wieckowski, and E. Oldfield, *J. Am. Chem. Soc.*, **124**, 468 (2002).
5. A. Lamouri, Y. Gofer, Y. Luo, G. S. Chottiner, and D. A. Scherson, *J. Phys. Chem. B*, **105**, 6172 (2001).
6. G. A. Camara, M. J. Giz, V. A. Paganin, and E. A. Ticianelli, *J. Electroanal. Chem.*, **537**, 21 (2002).
7. W. F. Lin, M. S. Zei, M. Eiswirth, G. Ertl, T. Iwasita, and W. Vielstich, *J. Phys. Chem. B*, **103**, 6968 (1999).
8. Z. Qi and A. Kaufman, *J. Power Sources*, **113**, 115 (2003).
9. R. Viswanathan, G. Hou, R. Liu, S. R. Bare, F. Modica, G. Mickelson, C. U. Segre, N. Leyarovska, and E. S. Smotkin, *J. Phys. Chem. B*, **106**, 3458 (2002).
10. C. Lu, C. Rice, R. I. Masel, P. K. Babu, P. Waszczuk, H. S. Kim, E. Oldfield, and A. Wieckowski, *J. Phys. Chem. B*, **106**, 9581 (2002).
11. M. T. M. Koper, N. P. Lebedeva, and C. G. M. Hermse, *Faraday Discuss.*, **121**, 301 (2002).
12. M. T. M. Koper, J. J. Lukkien, A. P. J. Jansen, and R. A. Van Santen, *J. Phys. Chem. B*, **103**, 5522 (1999).
13. M. T. M. Koper, T. E. Shubina, and R. A. van Santen, *J. Phys. Chem. B*, **106**, 686 (2002).
14. N. P. Lebedeva, M. T. M. Koper, J. M. Feliu, and R. A. van Santen, *J. Electroanal. Chem.*, **524–525**, 242 (2002).
15. C. Lu and R. I. Masel, *J. Phys. Chem. B*, **105**, 9793 (2001).
16. T. Yajima, H. Uchida, and M. Watanabe, *J. Phys. Chem. B*, **108**, 2654 (2004).
17. G. A. Camara, E. A. Ticianelli, S. Mukerjee, S. J. Lee, and J. McBreen, *J. Electrochem. Soc.*, **149**, A748 (2002).
18. S. Mukerjee and R. C. Urian, *Electrochim. Acta*, **47**, 3219 (2002).
19. R. C. Urian, A. F. Gulla, and S. Mukerjee, *J. Electroanal. Chem.*, **554–555**, 307 (2003).
20. S. J. Lee, S. Mukerjee, E. A. Ticianelli, and J. McBreen, *Electrochim. Acta*, **44**, 3283 (1999).
21. S. Mukerjee, R. C. Urian, S. J. Lee, E. A. Ticianelli, and J. McBreen, *J. Electrochem. Soc.*, **151**, A1094 (2004).
22. A. E. Russell, S. Maniguet, R. J. Mathew, J. Yao, M. A. Roberts, and D. Thompsett, *J. Power Sources*, **96**, 226 (2001).
23. P. Waszczuk, A. Wieckowski, P. Zelenay, S. Gottesfeld, C. Coutanceau, J. M. Leger, and C. Lamy, *J. Electroanal. Chem.*, **511**, 55 (2001).
24. G. Q. Lu, J. O. White, and A. Wieckowski, *Surf. Sci.*, **564**, 131 (2004).
25. G. Q. Lu, P. Waszczuk, and A. Wieckowski, *J. Electroanal. Chem.*, **532**, 49 (2002).
26. S. R. Brankovic, N. S. Marinkovic, J. X. Wang, and R. R. Adzic, *J. Electroanal. Chem.*, **532**, 57 (2002).
27. S. T. Kuk and A. Wieckowski, *J. Power Sources*, **141**, 1 (2005).
28. J. S. Spendelow, G. Q. Lu, P. J. A. Kenis, and A. Wieckowski, *J. Electroanal. Chem.*, **568**, 215 (2004).
29. W. F. Lin, T. Iwasita, and W. Vielstich, *J. Phys. Chem. B*, **103**, 3250 (1999).
30. M. S. McGovern, P. Waszczuk, and A. Wieckowski, *Electrochim. Acta*, **51**, 1194 (2006).
31. H. A. Gasteiger, N. Marković, P. N. Ross, Jr., and E. J. Cairns, *J. Phys. Chem.*, **98**, 617 (1994).
32. H. Massong, H. Wang, G. Samjeske, and H. Baltruschat, *Electrochim. Acta*, **46**, 701 (2000).
33. B. N. Grgur, N. M. Marković, and P. N. Ross, Jr., *J. Phys. Chem. B*, **102**, 2494 (1998).
34. B. N. Grgur, N. M. Marković, and P. N. Ross, *J. Electrochem. Soc.*, **146**, 1613 (1999).
35. B. N. Grgur, G. Zhuang, N. M. Marković, and P. N. Ross, Jr., *J. Phys. Chem. B*, **101**, 3910 (1997).
36. J. McBreen and S. Mukerjee, *J. Electrochem. Soc.*, **142**, 3399 (1995).
37. S. Mukerjee and J. McBreen, *J. Electrochem. Soc.*, **146**, 600 (1999).
38. M. T. M. Koper, *Surf. Sci.*, **548**, 1 (2004).
39. M. E. Gallagher, C. A. Lucas, V. Stamenkovic, N. M. Marković, and P. N. Ross, *Surf. Sci.*, **544**, L729 (2003).
40. Y. Morimoto and E. B. Yeager, *J. Electroanal. Chem.*, **444**, 95 (1998).
41. K. Wang, H. A. Gasteiger, N. M. Marković, and P. N. Ross, Jr., *Electrochim. Acta*, **41**, 2587 (1996).
42. H. A. Gasteiger, N. M. Marković, and P. N. Ross, Jr., *J. Phys. Chem.*, **99**, 8945 (1995).
43. M. T. Paffett, S. C. Gebhard, R. G. Windham, and B. E. Koel, *J. Phys. Chem.*, **94**, 6831 (1990).
44. A. N. Haner and P. N. Ross, *J. Phys. Chem.*, **95**, 3740 (1991).
45. N. M. Marković, A. Widelov, P. N. Ross, O. R. Monteiro, and I. G. Brown, *Catal. Lett.*, **43**, 161 (1997).
46. X.-Y. Xiao, S. Tillmann, and H. Baltruschat, *Phys. Chem. Chem. Phys.*, **4**, 4044 (2002).
47. V. R. Stamenkovic, M. Arenz, C. A. Lucas, M. E. Gallagher, P. N. Ross, and N. M. Marković, *J. Am. Chem. Soc.*, **125**, 2736 (2003).

48. B. E. Hayden, M. E. Rendall, and O. South, *J. Am. Chem. Soc.*, **125**, 7738 (2003).
49. M. Arenz, V. Stamenkovic, P. N. Ross, and N. M. Marković, *Electrochem. Commun.*, **5**, 809 (2003).
50. M. Goetz and H. Wendt, *J. Appl. Electrochem.*, **31**, 811 (2001).
51. D. C. Skelton, R. G. Tobin, D. K. Lambert, C. L. DiMaggio, and G. B. Fisher, *J. Phys. Chem. B*, **103**, 964 (1999).
52. M. Watanabe, M. Uchida, and S. Motoo, *J. Electroanal. Chem. Interfacial Electrochem.*, **229**, 395 (1987).
53. S. R. Brankovic, J. X. Wang, and R. R. Adzic, *Electrochem. Solid-State Lett.*, **4**, A217 (2001).
54. C. Roth, N. Benker, T. Buhrmester, M. Mazurek, M. Loster, H. Fuess, D. C. Koningsberger, and D. E. Ramaker, *J. Am. Chem. Soc.*, **127**, 14607 (2005).
55. E. Smotkin, E. Chung, S. Stoupin, S. Chattopadhyay, and C. U. Segre, Abstract 1559, The Electrochemical Society Meeting Abstracts, Quebec, Canada, May 15–20, 2005.
56. J. O'M. Bockris and H. Wroblowa, *J. Electroanal. Chem.*, **7**, 42851 (1964).
57. K. A. Friedrich, K. P. Geyzers, U. Linke, U. Stimming, and J. Stumper, *J. Electroanal. Chem.*, **402**, 123 (1996).
58. N. P. Lebedeva, M. T. M. Koper, J. M. Feliu, and R. A. van Santen, *J. Phys. Chem. B*, **106**, 12938 (2002).
59. N. P. Lebedeva, M. T. M. Koper, E. Herrero, J. M. Feliu, and R. A. van Santen, *J. Electroanal. Chem.*, **487**, 37 (2000).
60. N. P. Lebedeva, A. Rodes, J. M. Feliu, M. T. M. Koper, and R. A. van Santen, *J. Phys. Chem. B*, **106**, 9863 (2002).
61. S. Mukerjee, S. Srinivasan, and M. P. Soriaga, *J. Electrochem. Soc.*, **142**, 1409 (1995).
62. M. Teliska, W. E. O'Grady, and D. E. Ramaker, *J. Phys. Chem. B*, **108**, 2333 (2004).
63. M. Teliska, W. E. O'Grady, and D. E. Ramaker, *J. Phys. Chem. B*, **109**, 8076 (2005).
64. D. C. Koningsberger, J. de Graaf, B. L. Mojet, D. E. Ramaker, and J. T. Miller, *Appl. Catal., A*, **191**, 205 (2000).
65. B. L. Mojet, J. T. Miller, D. E. Ramaker, and D. C. Koningsberger, *J. Catal.*, **186**, 373 (1999).
66. D. E. Ramaker, B. L. Mojet, M. T. Garriga Oostenbrink, J. T. Miller, and D. C. Koningsberger, *Phys. Chem. Chem. Phys.*, **1**, 2293 (1999).
67. D. C. Koningsberger, M. K. Oudenhuijzen, J. H. Bitter, and D. E. Ramaker, *Top. Catal.*, **10**, 167 (2000).
68. B. L. Mojet, D. E. Ramaker, J. T. Miller, and D. C. Koningsberger, *Catal. Lett.*, **62**, 15 (1999).
69. D. E. Ramaker and D. C. Koningsberger, *Phys. Rev. Lett.*, **89**, 139701 (2002).
70. M. Teliska, V. S. Murthi, S. Mukerjee, and D. E. Ramaker, *J. Electrochem. Soc.*, **152**, A2159 (2005).
71. B. Ravel and M. Newville, *Synchrotron Radiat.*, **12**, 537 (2005).
72. M. Newville, P. Livins, Y. Yacoby, J. J. Rehr, and E. A. Stern, *Phys. Rev. B*, **47**, 14126 (1993).
73. M. Newville, *Synchrotron Radiat.*, **8**, 322 (2001).
74. S. I. Zabinsky, J. J. Rehr, A. Aukudinov, R. C. Albers, and M. J. Eller, *Phys. Rev. B*, **52**, 2995 (1995).
75. E. Janin, H. von Schenck, M. Gothelid, U. O. Karlsson, and M. Svensson, *Phys. Rev. B*, **61**, 13144 (2000).
76. I. Villegas and M. J. Weaver, *J. Chem. Phys.*, **101**, 1648 (1994).
77. N. M. Marković, C. A. Lucas, A. Rodes, V. Stamenkovic, and P. N. Ross, *Surf. Sci.*, **499**, L149 (2002).
78. D. C. Koningsberger and R. Prins, *X-Ray Absorption Spectroscopy: Theory, Techniques, and Applications*, John Wiley & Sons, New York (1988).
79. J. de Graaf, A. J. van Dillen, K. P. de Jong, and D. C. Koningsberger, *J. Catal.*, **203**, 307 (2001).
80. D. C. Koningsberger, B. I. Mojet, G. E. Van Dorssen, and D. E. Ramaker, *Top. Catal.*, **10**, 143 (2000).
81. N. Chakroune, G. Viau, S. Ammar, L. Poul, D. Veautier, M. M. Chehimi, C. Mangeney, F. Villain, and F. Fievet, *Langmuir*, **21**, 6788 (2005).
82. D. E. Ramaker, M. K. Oudenhuijzen, and D. C. Koningsberger, *J. Phys. Chem. B*, **109**, 5608 (2005).
83. B. J. Hwang, C.-H. Chen, L. S. Sarma, J.-M. Chen, G.-R. Wang, M.-T. Tang, D.-G. Liu, and J.-F. Lee, *J. Phys. Chem. B*, **110**, 6475 (2006).
84. J. X. Wang, N. M. Marković, and R. R. Adzic, *J. Phys. Chem. B*, **108**, 4127 (2004).
85. F. J. Scott, C. Roth, and D. E. Ramaker, *J. Phys. Chem.*, Submitted.
86. K. J. J. Mayrhofer, B. B. Blizanac, M. Arenz, V. R. Stamenkovic, P. N. Ross, and N. M. Marković, *J. Phys. Chem. B*, **109**, 14433 (2005).
87. S. Desai and M. Neurock, *Electrochim. Acta*, **48**, 3759 (2003).
88. J. W. Long, R. M. Stroud, K. E. Swider-Lyons, and D. R. Rolison, *J. Phys. Chem. B*, **104**, 9772 (2000).
89. H. Kim, I. Rabelo de Moraes, G. Tremiliosi-Filho, R. Haasch, and A. Wieckowski, *Surf. Sci.*, **474**, L203 (2001).
90. C. Bock, M. A. Blakely, and B. MacDougall, *Electrochim. Acta*, **50**, 2401 (2005).
91. C. Bock, A. Collier, and B. MacDougall, *J. Electrochem. Soc.*, **152**, A2291 (2005).
92. T. Frelink, W. Visscher, A. P. Cox, and J. A. R. van Veen, *Ber. Bunsenges. Phys. Chem.*, **100**, 599 (1996).
93. H. Hoster, T. Iwasita, H. Baumgartner, and W. Vielstich, *Phys. Chem. Chem. Phys.*, **3**, 337 (2001).
94. T. Iwasita, F. C. Nart, B. Lopez, and W. Vielstich, *Electrochim. Acta*, **37**, 2361 (1992).
95. T. Iwasita, H. Hoster, A. John-Anacker, W. F. Lin, and W. Vielstich, *Langmuir*, **16**, 522 (2000).
96. X. H. Xia, T. Iwasita, F. Ge, and W. Vielstich, *Electrochim. Acta*, **41**, 711 (1996).
97. K. Sasaki, J. X. Wang, M. Balasubramanian, J. McBreen, F. Uribe, and R. R. Adzic, *Electrochim. Acta*, **49**, 3873 (2004).
98. K. Sasaki, Y. Mo, J. X. Wang, M. Balasubramanian, F. Uribe, J. McBreen, and R. R. Adzic, *Electrochim. Acta*, **48**, 3841 (2003).
99. J. X. Wang, S. R. Brankovic, Y. Zhu, J. C. Hanson, and R. R. Adzic, *J. Electrochem. Soc.*, **150**, A1108 (2003).
100. P. K. Babu, H. S. Kim, S. T. Kuk, J. H. Chung, E. Oldfield, A. Wieckowski, and E. S. Smotkin, *J. Phys. Chem. B*, **109**, 17192 (2005).
101. C. Bock, B. MacDougall, and Y. LePage, *J. Electrochem. Soc.*, **151**, A1269 (2004).
102. F. J. Scott, S. Mukerjee, and D. E. Ramaker, *J. Electrochem. Soc*., Submitted.